

Structure of von Willebrand factor A1 on polystyrene determined from experimental and calculated sum frequency generation spectra

Steven J. Roeters,¹ Elaine H. Tronic,² Joe E. Baio,³ David G. Castner,² and Tobias Weidner^{1,a)}

¹Department of Chemistry, Aarhus University, 8000 Aarhus C, Denmark

²Departments of Bioengineering & Chemical Engineering, National ESCA & Surface Analysis Center for Biomedical Problems (NESAC/BIO), University of Washington, Box 351653, Seattle, Washington 98195-1653

³School of Chemical, Biological and Environmental Engineering, Oregon State University, Corvallis, Oregon 97331

(Received 13 September 2018; accepted 13 November 2018; published 14 December 2018)

The blood-clotting protein von Willebrand factor (vWF) can be activated by small molecules, high shear stress, and interactions with interfaces. It subsequently binds platelet receptor glycoprotein Ib α (GPIb α) at the surface of platelets, thereby playing a crucial role in blood clotting due to platelet activation, which is an important process to consider in the design of cardiovascular implants and biomaterials used in blood-contacting applications. The influence of surfaces on the activation and the molecular-level structure of surface-bound vWF is largely unknown. Recent studies have indicated that when bound to hydrophobic polystyrene (PS), the A1 domain of vWF remains accessible for GPIb α binding. However, the detailed secondary structure and exact orientation of vWF A1 at the PS surface is still unresolved. Here, the authors resolve these features by studying the system with sum-frequency generation (SFG) spectroscopy. The data are consistent with a scenario where vWF A1 maintains a native secondary structure when bound to PS. Comparison of experimental and calculated SFG spectra combined with previously reported time-of-flight secondary ion mass spectrometry data suggests that A1 assumes an orientation with the GPIb α binding domain oriented away from the solid surface and exposed to the solution phase. This structural information will benefit future *in vitro* experiments with surface-adsorbed A1 domain and may have relevance for the design of novel blood-contacting biomaterials and wound-healing applications. Published by the AVS. <https://doi.org/10.1116/1.5056219>

I. INTRODUCTION

When proteins attach to a material surface, they guide material-biological interactions and act as the interface between the biological environment and the material.^{1,2} When a material is in contact with blood, rapid attachment of specific plasma proteins to the material surface^{3,4} results in the adhesion of platelets and, consequently, their activation, which finally can lead to thrombosis.⁵ Given sufficient time, this process also takes place at the surface of implanted biomedical materials such as stents, in spite of many attempts to prevent adverse biological reactions.^{4,5} One attempt at preventing platelet activation that has been partially successful is the administration of blood thinners, but this typically only slows down platelet activation or prevents re-endothelialization of the material surface, leading to delayed thrombosis events.⁶ Platelet activation could in principle be regulated by the control of platelet–surface interactions at the molecular level. However, this strategy would have to be based on a detailed understanding of the different signaling pathways involved in platelet activation from circulating plasma proteins and plasma proteins immobilized on a synthetic surface.

Von Willebrand factor (vWF) is a particularly important protein in this context. vWF is implicated in cardiovascular

disease,^{7,8} and the protein has been applied as an indicator of the severity of acute cases of blood-vessel blockages.⁹ Multimeric vWF is a large (>20 000 kDa) polymerized aggregate of several vWF monomers.¹⁰ The vWF monomer consists of subunit domains with specific functions. The A1 domain of vWF is of particular importance for platelet-surface interactions since it can initiate the binding to the platelet receptor glycoprotein Ib α (GPIb α).^{11–15} vWF acts as a sensor for blood-vessel damage when circulating in the blood. Superphysiological levels of shear stress will activate vWF [e.g., 100 dynes/cm² (Refs. 16–20)]. GPIb α binding to A1 activates integrin and, subsequently, formation of a stable thrombus.²¹ In addition, vWF can bind to exposed collagen on injured tissue and mediate platelet adhesion even under high shear stresses that are too high for other blood-related proteins such as fibrinogen.^{22,23}

Consequently, vWF plays a key role for the biological response to blood-related biomaterial implants and thrombotic response. At the same time, the interactions between GPIb α and the A1 domain when vWF is bound to a surface are poorly understood. It is currently debated whether the mechanism is based on the exposure of the GPIb α binding domain,^{22,24} destabilization of the native A1 secondary and tertiary structure,^{15,25–27} or stretching the structure of vWF in the blood flow and activation of catch bonds.^{28–31} For a better understanding of the surface interactions of A1, Tronic *et al.* have used a range of complementary surface analysis

^{a)}Author to whom correspondence should be addressed: weidner@chem.au.dk

techniques to determine the interaction of vWF with a set of hydrophilic and hydrophobic surfaces.³² X-ray photoelectron spectroscopy, time-of-flight secondary ion mass spectrometry (ToF-SIMS), and near-edge x-ray absorption fine structure data in combination with enzyme-linked immunosorbent assay and platelet adhesion assays showed that vWF interactions are strongly correlated with the surface chemistry.

A comparison of the vWF interaction with hydrophilic glass and hydrophobic polystyrene (PS) surfaces showed that at high flow rates (typical for blood vessel damage), PS-adsorbed A1 mediated stronger platelet adhesion than A1 bound to glass. It was concluded that the biological function of A1 adsorbed onto PS is typical of native vWF, while the biological impact of A1 adsorbed onto glass was more typical of alternate A1 structures that retain ability to bind specifically to platelet GPIb α , but with altered, nonnative folding and conformation. However, while this previous investigation provides a general picture of the protein's surface structure, the exact orientation and details about the secondary structure of A1 could not be obtained. For a more detailed picture of A1, we have analyzed the surface folding using sum-frequency generation (SFG) vibrational spectroscopy. SFG amide-I spectroscopy has in recent years been developed into a tool to determine the protein secondary structure and orientation at interfaces.^{33–36} Owing to its surface sensitivity, it is ideally suited to probe monolayers of proteins at surfaces. A detailed spectral analysis can be obtained by comparison with theoretical spectra calculated from simulated structures^{37,38} or previously-determined structure data.^{39,40}

In this study, we have probed vWF A1 on PS surfaces because of its high relevance as a model system for hydrophobic biomedical surfaces. To extract structural information from the SFG dataset, we have combined the experimental data with theoretical spectra calculated from x-ray diffraction data.

II. METHODS

A. vWF A1 binding and substrate preparation

Polystyrene films were fabricated by spin-casting a 3% solution (wt./wt. in toluene) of PS (Polymer Source Inc.) onto one side of an equilateral CaF₂ prism at 3000 rpm. The PS film was then brought into contact with a 1× phosphate buffered saline (PBS) solution and the interface was probed through the backside of the film. A1, generously provided by

Miguel Cruz, was produced in *E. coli* containing residues 1238–1472 of mature vWF with 12 residues at the N terminus from the expression vector (MRGSHHHHHGS).⁴¹ The buffer was replaced by the A1 solution without exposing the PS surface to air. The concentration of the A1 solution used in this study was 0.5 mg/ml.

B. Sum-frequency generation spectroscopy

Details of the SFG setup are published elsewhere⁴² and will only be briefly discussed here. In short, the visible beam with a wavelength of 532 nm was delivered by an EKSPLA Nd:YAG laser operating at 50 Hz, which was also used to pump an EKSPLA optical parametric generation/amplification and difference-frequency unit based on barium borate and AgGaS₂ crystals to generate tunable infrared (IR) laser radiation from 1000 to 4000 cm⁻¹. The bandwidth was 2 cm⁻¹ for the visible pump pulses and 6 cm⁻¹ for the IR laser. Both beams were focused at the sample with energies of 150 and 200 μJ per pulse for the visible and the IR beam, respectively. The spectra were collected with 200 shots per data point in 2 cm⁻¹ increments. The SFG spectra were normalized by the product of the IR and visible pump beam intensities. The incident angles of the visible and IR pump beams inside the prism were 47° and 58° versus the surface normal of the PS interface, respectively.

C. SFG spectra calculations

The spectral calculation is based on the formalism published in Ref. 35. In short, we construct a one-exciton Hamiltonian for the amide-I mode of the backbone amide groups in the protein, with a single local-mode frequency (i.e., assuming that, on average, all amide groups are hydrogen-bonded equally) and couplings that are modeled differently for nearest- and nonnearest-neighbor amide groups. The nearest-neighbor interactions, dominated by through-bond effects, are modeled using a parameterized map of an *ab initio* calculation with the 6-31G+(d) basis set and the B3LYP functional, which gives the coupling as a function of the dihedral angle.^{43,44} The nonnearest-neighbor interactions, dominated by through-space effects, are modeled using the transition-dipole coupling model.⁴⁵ The Hamiltonian is then diagonalized to obtain the amide-I eigenvalues and eigenvectors, from which the spectroscopic response is calculated. To account for the azimuthal isotropy of the proteins at the interface, we average the Euler angle ϕ [see Fig. 1(b)] from 0 to 2π .

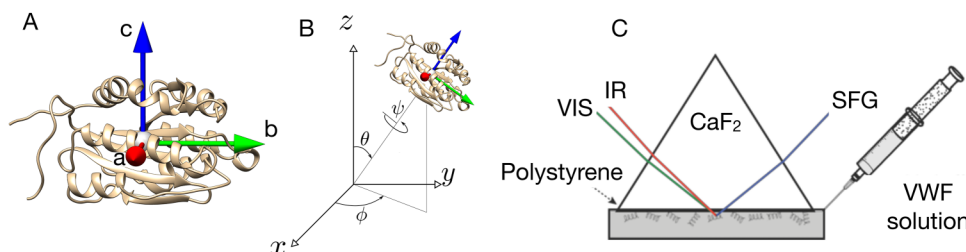


Fig. 1. Molecular frame and experimental setup. (a) The axes are determined with the orient of protein orientation in the laboratory frame. (c) Experimental setup for *in situ* SFG measurements of vWF A1-PS binding.

We performed a grid search over the other two Euler angles, Θ and ψ , to find the minimum in the residual sum of squares (RSS) between the calculated and experimental spectra in the ssp and ppp polarization combinations (using a single, overall scaling factor for both polarization combinations). In total, we calculated $\sim 10\,000$ spectra for this, varying Θ from 0 to 180° and ψ from 0 to 360° , both with a resolution of 2.5° . We then performed a free fit in Θ and ψ near the RSS minimum to obtain the optimal angles of **Or1** and **Or2** (see Sec. III). We model the local-field corrections as described in Ref. 46, for which we have assumed the refractive index of bulk PS for the layer above the interface, using the dispersion relation reported in Ref. 47 (leading to $n_{1,SF} = 1.60$, $n_{1,VIS} = 1.60$, and $n_{1,IR} = 1.56$ at the employed frequencies of ~ 490 , 532, and ~ 6000 nm for the sum-frequency (SF), VIS, and IR fields, respectively), the refractive index typical for bulk protein solutions⁴⁸ for the interfacial refractive indices (leading to $n_i = 1.32$ at all frequencies, because the dispersion is almost negligible for proteins⁴⁹), and the refractive index of bulk H₂O (Ref. 50) for the layer below the surface (leading to $n_{2,SF} = 1.34$, $n_{2,VIS} = 1.34$, and $n_{2,IR} = 1.27$). An optimal match between calculations and experiment was found for a central frequency (the gas phase frequency minus an overall frequency shift due to hydrogen bonding) of 1651 cm^{-1} , which is in line with previous calculations using the same method,^{51,53} and a Lorentzian width of 6 cm^{-1} , which is in line with the experimentally determined linewidth of the IR beam.

III. RESULTS

To determine the orientation of vWF A1 [Figs. 1(a) and 1(b)] on PS, we recorded SFG spectra from A1 *in situ* in PBS buffer. A schematic of the sample cell is depicted in Fig. 1(c). The PS–protein–buffer interface was probed going through the backside of a CaF₂ prism. Experimental SFG amide-I spectra collected in ssp (s-polarized SFG, s-polarized VIS, p-polarized IR) and ppp polarization combinations are shown in Fig. 2(a). Both ssp and ppp spectra are dominated by a strong feature near 1640 cm^{-1} . A shoulder near 1625 cm^{-1} is also visible in both spectra. These resonances are

commonly assigned to β -sheet secondary structures. A weak shoulder observed near 1650 cm^{-1} typically is related to α -helical or random folds. Both secondary structure motifs are present in the native A1 domain (Fig. 1). If the β -sheet and α -helical secondary structures were denatured on the surface, no peaks would be observed in the SFG spectra.

Protein SFG spectra are heavily influenced by interference between signals from different secondary-structure elements and protein sidechains, based on their relative orientation and energy. For small proteins and peptides, the direct analysis of SFG amide-I spectra by peak fitting can provide information about the orientation and structure.^{33,34,52} However, since the A1 structure is complex, which leads to severe spectral interference and convolution, it is not possible to obtain unambiguous information about the protein conformation by direct spectral inspection and fitting. To solve this problem and to make full use of the structural information within the SFG spectra, we have developed a framework for calculating theoretical SFG spectra from protein data bank (PDB)^{35,39,54} and molecular dynamics structure files.^{37,38,51} Thus, spectra for this study were calculated from PDB models. In addition, by calculating spectra for different protein orientations with respect to the surface and matching experimental and calculated spectra for different orientations, one can determine the surface binding geometry.

Figure 2(a) shows theoretical SFG spectra calculated for the crystal structure of vWF A1 (PDB-entry 1AUQ) for a tilt angle $\Theta = 68^\circ$ and a twist angle $\psi = 97^\circ$ (orientation abbreviated **Or1**). Besides the overall intensity and orientation, no adjustable parameters were used to match the calculated spectra to the experimental data. The calculations match the experimental spectral features very well [RSS < 1.2; see Fig. 2(b)], with a main resonance near 1640 cm^{-1} along with shoulders near 1625 and 1650 cm^{-1} . Importantly, the relative intensities of ssp and ppp spectra match the experimental data. The agreement of experimental and calculated spectra clearly indicates that vWF A1 maintains a folding structure close to its native state when bound to PS.

The question arises how unique the spectral match is for the set of tilt and twist angles. The orientation of the A1

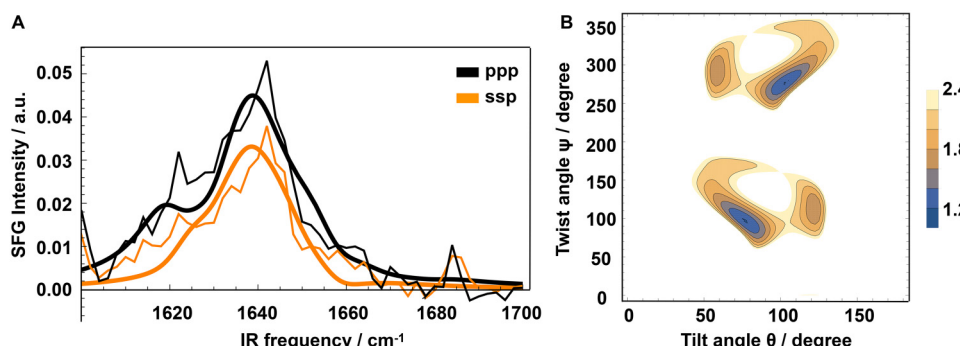


FIG. 2. Comparison of experimental and calculated SFG spectra. (a) Thin lines: Experimental spectra collected for ssp and ppp polarization combinations. Thick lines: Spectra calculated from the XRD structure 1AUQ for a tilt angle of 68° and a twist angle of 97° . (b) RSS plot representative for the experimental fitness of SFG spectra calculations for different sets of theta and phi angles of vWF at a polystyrene surface. The white area indicates the region where the RSS values are larger than 2.4.

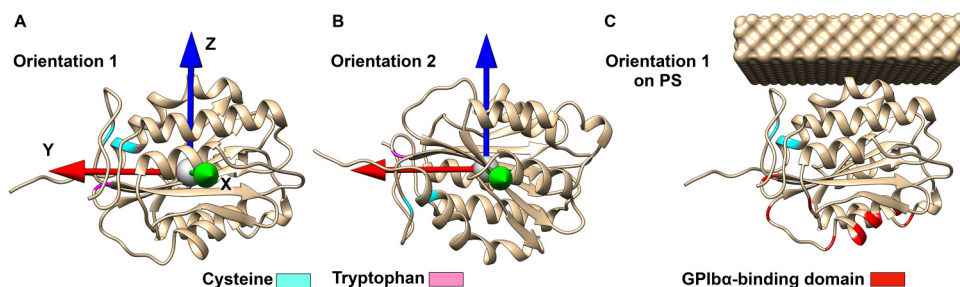


Fig. 3. Orientations extracted from the raster search. (a) and (b) Orientations **Or1** and **Or2** for vWF A1 on polystyrene surfaces for SFG spectra calculations show significant spectral match with experimental spectra. Cysteine and tryptophan residues are marked in cyan and pink, respectively. (c) Orientation of the GPIba binding domain in **Or1** (marked in red) with respect to the PS surface—see Fig. 1(c) for the sample geometry.

domain was therefore determined by a systematic grid search using varied tilt and twist angles. The RSS values were determined by comparing a total of $\sim 10\,000$ calculated spectra with the experimental spectra. The results of the search are summarized in Fig. 2(b). The 2D plot shows two regions with protein orientations that resulted in a significant match between theory and experiment. Besides the orientation discussed above, there is a second region of orientations with a similar experimental fitness around $\Theta = 112^\circ$ and a twist angle $\psi = 277^\circ$ (abbreviated **Or2**). The orientations **Or1** and **Or2** are shown in Figs. 3(a) and 3(b). Note that the homodyne SFG signal for a given set of (Θ, ψ) -values equals that of $(180 - \Theta, 180 + \psi)$ for an azimuthal isotropy. Therefore, the experimental SFG data are reproduced equally well for **Or1** and **Or2**, while the orientations are dramatically different. In fact, the GPIba binding domain [marked in red in Fig. 3(c)] orients away from the PS surface in **Or1** while it is oriented toward the PS surface in **Or2**. Thus, A1 GPIba binding domain in the **Or2** orientation would not be accessible to GPIba.

Previously reported ToF-SIMS analysis of the relative positions of key amino acids can provide the additional information needed to determine which of the two proposed scenarios from SFG represents the more likely binding geometry. ToF-SIMS provides information about the presence of amino acids within the outermost ~ 2 nm of an adsorbed protein layer, which can be used to determine differences in orientation or even conformation for rare or asymmetrically distributed amino-acid sequence between protein layers.^{54,55} The relative location of the Cys residues which stabilize the A1 domain by connecting the N- and C-termini is particularly helpful here. Tronic *et al.* have shown that the Cys residues are less exposed on PS, i.e., closer to the PS surface, compared with hydrophilic surfaces. At the same time, residue Trp1313 (of full-length vWF—when counting from the first residue of the mature subunit as in Ref. 13, this is residue Trp550) was more exposed, i.e., further away from the PS surface compared with the glass surface. The respective Cys and Trp sites are marked in cyan and pink, respectively, for the two candidate states **Or1** and **Or2** depicted in Figs. 3(a) and 3(b). Clearly, **Or1**, with the Cys units closer to the PS surface than the Trp site, matches the previously reported ToF-SIMS data. In this orientation,

the GPIba binding site (as determined with x-ray crystallography¹³) is pointing away from the PS surface where it is exposed to the surrounding solution and can effectively interact with the glycoprotein.

IV. CONCLUSIONS

The present study is an excellent example for the need to combine multiple surface analytical techniques to provide a more detailed understanding of a protein's surface state. By comparing experimental and calculated SFG spectra, we have investigated the conformation and orientation of vWF A1 adsorbed onto PS. The SFG results clearly show that the A1 domain remains intact and binds in a native state to PS. By combining SFG with previously reported ToF-SIMS data, we can conclude that vWF A1 orients with the GPIba binding domain exposed to the solution and accessible for platelet binding. This finding supports the hypothesis that vWF mediates effective attachment of platelets to hydrophobic surfaces by the presentation of the intact GPIba binding motif to platelet binding sites. Together, the results provide a first molecular level picture of the secondary structure and orientation of vWF A1 on surfaces.

ACKNOWLEDGMENTS

These studies were supported by the National Institutes of Health (Grant No. EB-002027, National ESCA and Surface Analysis Center for Biomedical Problems). E.H.T. was supported by the National Science Foundation Graduate Research Fellowship Program. S.J.R. and T.W. thank the Aarhus Research Foundation (AUFF), Villum Fonden, and the Deutsche Forschungsgemeinschaft (DFG Grant No. WE4478/4-1) for financial support.

¹D. G. Castner and B. D. Ratner, *Surf. Sci.* **500**, 28 (2002).

²D. G. Castner, *Biointerphases* **12**, 02C301 (2017).

³B. Young, L. Lambrecht, S. Cooper, and D. Mosher, *Adv. Chem. Ser.* **199**, 317 (1982).

⁴J. Brash and T. Horbett, *ACS Symp. Ser.* **602**, 1 (1995).

⁵M. B. Gorbet and M. V. Sefton, *Biomaterials* **25**, 5681 (2004).

⁶M. Jone *et al.*, *J. Am. Coll. Cardiol.* **48**, 193 (2006).

⁷C. M. Gibson, L. Diaz, K. Kandarpa, F. M. Sacks, R. C. Pasternak, T. Sandor, C. Feldman, and P. H. Stone, *Arterioscler. Thromb.* **13**, 310 (1993).

⁸L. D. Back, J. R. Radbill, and D. W. Crawford, *J. Biomech.* **10**, 339 (1977).

- ⁹P. Paulinska, A. Spiel, and B. Jilma, *Hamostaseologie* **29**, 32 (2009).
- ¹⁰P. Lenting and C. Denis, *J. Thromb. Haemost.* **5**, 1361 (2007).
- ¹¹S. Miura, C. Q. Li, Z. Cao, H. Wang, M. R. Wardell, and J. E. Sadler, *J. Biol. Chem.* **275**, 7539 (2000).
- ¹²J. J. Dumas, R. Kumar, T. McDonagh, F. Sullivan, M. L. Stahl, W. S. Somers, and L. Mosyak, *J. Biol. Chem.* **279**, 23327 (2004).
- ¹³E. G. Huizinga, S. Tsuji, R. A. Romijn, M. E. Schiphorst, P. G. de Groot, J. J. Sixma, and P. Gros, *Science* **297**, 1176 (2002).
- ¹⁴M. A. Cruz, T. G. Diacovo, J. Emsley, R. Liddington, and R. I. Handin, *J. Biol. Chem.* **275**, 19098 (2000).
- ¹⁵H. Ulrichs, M. Udvardy, P. J. Lenting, I. Pareyn, N. Vandepitte, K. Vanhoorebeke, and H. Deckmyn, *J. Biol. Chem.* **281**, 4699 (2006).
- ¹⁶B. Savage, E. Saldivar, and Z. M. Ruggeri, *Cell* **84**, 289 (1996).
- ¹⁷M. Sugimoto, S. Tsuji, M. Kuwahara, H. Matsui, S. Miyata, Y. Fujimura, and A. Yoshioka, *Int. J. Hematol.* **69**, 48 (1999).
- ¹⁸Y. P. Wu, T. Vink, M. Schiphorst, G. H. van Zanten, I. J. MJ, P. G. de Groot, and J. J. Sixma, *Arterioscler. Thromb. Vasc. Biol.* **20**, 1661 (2000).
- ¹⁹S. Goto, Y. Ikeda, E. Saldivar, and Z. M. Ruggeri, *J. Clin. Invest.* **101**, 479 (1998).
- ²⁰H. Shankaran, P. Alexandridis, and S. Neelamegham, *Blood* **101**, 2637 (2003).
- ²¹D. A. Beacham, R. J. Wise, S. M. Turci, and R. I. Handin, *J. Biol. Chem.* **267**, 3409 (1992).
- ²²S. W. Schneider, S. Nuschele, A. Wixforth, C. Gorzelanny, A. Alexander-Katz, R. R. Netz, and M. F. Schneider, *Proc. Natl. Acad. Sci. U.S.A.* **104**, 7899 (2007).
- ²³L. Novák, H. Deckmyn, S. Damjanovich, and J. Hársfalvi, *Blood* **99**, 2070 (2002).
- ²⁴P. J. Lenting, J. N. Pegon, E. Groot, and P. G. Groot, *Thromb. Haemost.* **104**, 449 (2010).
- ²⁵C. A. Siedlecki, B. J. Lestini, K. K. Kottke-Marchant, S. J. Eppell, D. L. Wilson, and R. E. Marchant, *Blood* **88**, 2939 (1996).
- ²⁶J. F. Dong, M. C. Berndt, A. Schade, L. V. McIntire, R. K. Andrews, and J. A. Lopez, *Blood* **97**, 162 (2001).
- ²⁷O. J. McCarty, S. Calaminus, M. Berndt, L. Machesky, and S. Watson, *J. Thromb. Haemost.* **4**, 1367 (2006).
- ²⁸T. Yago et al., *J. Clin. Invest.* **118**, 3195 (2008).
- ²⁹W. E. Thomas, R. A. Penkala, E. Hillenmeyer, M. Whitfield, A.-y. Tu, A. D. Munday, P. J. Lenting, J. Kulman, and J. A. López, *Blood* **116**, 2117 (2010).
- ³⁰W. E. Thomas, B. Penkala, M. Whitfield, A.-Y. Tu, A. Munday, J. Kulman, and J. A. López, *Biophys. J.* **100**, 480a (2011).
- ³¹G. Interlandi and W. Thomas, *Proteins* **78**, 2506 (2010).
- ³²E. H. Tronic, O. Yakovenko, T. Weidner, J. E. Baio, R. Penkala, D. G. Castner, and W. E. Thomas, *Biointerphases* **11**, 029803 (2016).
- ³³K. T. Nguyen, S. V. Le Clair, S. Ye, and Z. Chen, *J. Phys. Chem. B* **113**, 12169 (2009).
- ³⁴K. T. Nguyen, J. T. King, and Z. Chen, *J. Phys. Chem. B* **114**, 8291 (2010).
- ³⁵S. J. Roeters, C. N. van Dijk, A. Torres-Knoop, E. H. G. Backus, R. K. Campen, M. Bonn, and S. Woutersen, *J. Phys. Chem. A* **117**, 6311 (2013).
- ³⁶E. C. Yan, L. Fu, Z. Wang, and W. Liu, *Chem. Rev.* **114**, 8471 (2014).
- ³⁷H. Lu, H. Lutz, S. J. Roeters, M. A. Hood, A. Schäfer, R. Muñoz-Espí, R. Berger, M. Bonn, and T. Weidner, *JACS* **140**, 2793 (2018).
- ³⁸D. Schach et al., *J. Phys. Chem.* **141**, 22D517 (2014).
- ³⁹R. Hennig et al., *Nat. Commun.* **6**, 7018 (2015).
- ⁴⁰C. Bernhard, S. J. Roeters, J. Franz, T. Weidner, M. Bonn, and G. Gonella, *Phys. Chem. Chem. Phys.* **19**, 28182 (2017).
- ⁴¹J. Emsley, M. Cruz, R. Handin, and R. Liddington, *J. Biol. Chem.* **273**, 10396 (1998).
- ⁴²J. Baio, T. Weidner, J. Brison, D. Graham, L. J. Gamble, and D. G. Castner, *J. Electron. Spectrosc. Relat. Phenom.* **172**, 2 (2009).
- ⁴³R. D. Gorbunov, D. S. Kosov, and G. Stock, *J. Chem. Phys.* **122**, 224904 (2005).
- ⁴⁴P. Hamm and M. Zanni, *Concepts and Methods of 2D Infrared Spectroscopy* (Cambridge University, New York, 2011).
- ⁴⁵S. Krimm and J. Bandekar, *Adv. Protein Chem.* **38**, 181 (2018).
- ⁴⁶X. Zhuang, P. Miranda, D. Kim, and Y. Shen, *Phys. Rev. B* **59**, 12632 (1999).
- ⁴⁷N. Sultanova, S. Kasarova, and I. Nikolov, *Acta Phys. Pol. A* **116**, 585 (2009).
- ⁴⁸D. B. Hand, *J. Biol. Chem.* **108**, 703 (1935).
- ⁴⁹A. Bucciarelli, V. Mulloni, D. Maniglio, R. Pal, V. Yadavalli, A. Motta, and A. Quaranta, *Opt. Mater.* **78**, 407 (2018).
- ⁵⁰G. M. Hale and M. R. Querry, *Appl. Opt.* **12**, 555 (1973).
- ⁵¹L. Schmüser, S. Roeters, H. Lutz, S. Woutersen, M. Bonn, and T. Weidner, *J. Phys. Chem. Lett.* **8**, 3101 (2017).
- ⁵²Y. Liu, J. Tan, J. Zhang, C. Li, Y. Luo, and S. Ye, *Chem. Commun.* **54**, 5903 (2018).
- ⁵³D. Verreault, S. Alamdari, S. J. Roeters, R. Pandey, J. Pfaendtner, and T. Weidner, *PCCP* **20**, 26926 (2018).
- ⁵⁴L. A. Scudeller, S. Srinivasan, A. M. Rossi, P. S. Stayton, G. P. Drobny, and D. G. Castner, *Biointerphases* **12**, 02D411 (2017).
- ⁵⁵R. Michel and D. G. Castner, *Surf. Interface Anal.* **38**, 1386 (2006).